forests

MDPI

Article

Greenness, Growth and Productivity in Die-Off Sites Indicate Drought Sensitivity in Semi-Arid Forests and Rapid Recovery

Arens Pëto [1], Antonio Gazol [1], Cristina Valeriano [1,2], Michele Colangelo [3], Manuel Pizarro [1], Ester González de Andrés [1,2], Jie Li [4], Xiaoxia Li [4] and Jesús Julio Camarero [1,*]

[1] Instituto Pirenaico de Ecología (IPE-CSIC), Avda. Montañana 1005, E-50192 Zaragoza, Spain; rensipeto@gmail.com (A.P.); agazol@ipe.csic.es (A.G.); valeriac@natur.cuni.cz (C.V.); m.pizarro@csic.es (M.P.); gonzalees@natur.cuni.cz (E.G.d.A.)
[2] Department of Physical Geography and Geoecology, Faculty of Science, Charles University, Albertov 6, 12843 Prague, Czech Republic
[3] Dipartimento di Scienze Agrarie, Forestali, Alimentari e Ambientali, Università della Basilicata, 85100 Potenza, Italy; michele.colangelo@unibas.it
[4] State Key Laboratory of Tibetan Plateau Earth System, Environment and Resources (TPESER), Institute of Tibetan Plateau Research, Chinese Academy of Sciences, Beijing 100101, China; lijie@itpcas.ac.cn (J.L.); lxx@itpcas.ac.cn (X.L.)
* Correspondence: jjcamarero@ipe.csic.es

Abstract

Aridification and hotter droughts are triggering forest die-off events characterized by high mortality rates and declines in forest productivity. The western Mediterranean Basin is a climate change hotspot where many of these die-off events have affected several tree and shrub species in recent decades. Yet, the responses of canopy greenness and cover, radial growth, and gross primary productivity (GPP) to climate in these die-off sites remain poorly understood across species and biomes. Here, we examined 44 sites across Spain, covering humid, dry sub-humid, and semi-arid biomes, and including nine tree and one shrub species. We obtained and correlated monthly climate data, satellite-derived vegetation indices (Normalized Difference Vegetation Index, Enhanced Vegetation Index), tree-ring metrics (basal area increment, ring-width indices), and GPP. We assessed climate trends and relationships between climate, vegetation indices, growth, GPP, and resilience after five extreme drought years in the period 1984–2023. Climate warming impacted all sites, increasing vapor pressure deficit and reducing soil moisture availability, with semi-arid sites warming the most. Vegetation indices and growth showed the largest declines during extreme droughts in dry sub-humid and semi-arid sites. Correlations with climate variables highlighted strong sensitivity to drought stress, particularly regarding growth metrics. During die-off events, GPP significantly declined in the growing season, but no legacy effects were observed afterwards. Vegetation indices and growth partially recovered one year after drought, with resilience peaking for GPP in semi-arid sites. Hotter droughts constrain GPP and growth, especially in dry sub-humid and semi-arid forests. Forests and shrublands experiencing die-off are diagnostic monitors of drought-induced thresholds in ecosystem productivity.

Keywords: dendroecology; dieback; forest productivity; vapor pressure deficit

Academic Editor: Algirdas Augustaitis

Received: 17 May 2026
Revised: 10 June 2026
Accepted: 11 June 2026
Published: 17 June 2026

1. Introduction

Climate warming is causing an intensification of drought severity worldwide by increasing atmospheric evaporative demand and reducing soil moisture [1,2]. Climate change is

leading to the occurrence of more severe periods of water scarcity that occur in combination with hotter temperatures, leading to the emergence of compound climate events referred to as 'hotter droughts', linked to forest die-off events and elevated tree mortality rates [3–6]. One of the regions most affected by such a warming and drying trend is the Mediterranean Basin, which has been considered a climate change hotspot [7]. In this region, aridification and intensified drought stress have negatively impacted forest productivity, canopy greenness, and tree growth, causing numerous die-off events affecting both conifers and broadleaves [8–11]. These die-off sites, where drought has triggered growth decline and high mortality rates surpassing resilience thresholds, have attracted the interest of researchers, managers and local stakeholders. However, resilience assessments based on canopy greenness derived from satellite imagery have revealed forest encroachment and rapid post-drought recovery in Mediterranean forested countries such as Spain [12], and also globally [13]. In other words, local die-off events, characterized by growth decline, mortality and vegetation browning, occur within a background of broad-scale greening.

How hotter droughts impact forest productivity, growth and greenness depends on multiple factors, including site climate conditions, tree functional groups (e.g., conifers, broadleaves), soil properties, topography, stand structure, disturbances, and resilience capacity, among other variables [8]. Examining these responses, considering several variables across wide environmental and climatic gradients, and focusing on die-off sites, where drought has triggered growth decline and high mortality rates, should provide relevant information on how forests recover after severe water shortage and elevated temperatures. Nevertheless, integrating satellite-derived vegetation indices with site growth data (tree-ring metrics) is challenging due to spatial and temporal mismatches and because foliage and wood production respond to different climate stressors [14].

First, there have been several reviews and studies on the use of remote sensing data to assess changes in forest health [14–16], but few of them focused on die-off sites [13]. Second, some of these studies focused on forest decline and die-off but combined vegetation indices and tree-ring data [17,18]. This combination has produced numerous papers showing very different responses depending on biomes, tree species, forest structure and the Vegetation Index considered [19–23]. Third, those studies using remote-sensing and tree-ring data were recently reviewed, highlighting that forest responses, in terms of a reduction in canopy cover or greenness and growth, often strengthen in seasonally dry and sensitive sites, particularly semi-arid forests [24]. Nevertheless, few studies, e.g., [11] have considered drought-induced die-off sites and how forest recovery proceeds afterwards in terms of canopy cover or greenness and tree growth. One recent research investigated the impacts of hotter droughts on a satellite-based Vegetation Index (Normalized Difference Vegetation Index, NDVI) and gross primary production (GPP) in die-off sites [25]. They reported that (i) 60%–80% of the die-off sites showed declines in NDVI and GPP at fine to moderate (30–500 m) resolutions, and (ii) the impacts of drought depended on temperature and vapor pressure deficit (VPD). Therefore, drought-induced die-off not only alters vegetation dynamics, but may also constrain the carbon uptake of forests and compromise their potential to partially mitigate climate warming. There is still, however, a research gap involving critical comparisons between satellite-derived information (NDVI, GPP) and field-based measures of tree growth, which would improve our detection and assessment of die-off and mortality impacts across different biomes, considering different tree and even shrub species.

Here, we aim to address this research gap by studying the responses to hotter droughts of 10 tree and shrub species located in 44 forest die-off sites sampled across Spain and encompassing humid to semi-arid climate conditions. We aim to (i) assess the long-term changes in climate conditions, canopy cover and greenness, radial growth and GPP and quantify how they are correlated, (ii) evaluate the influences of climate variables on those

forest response variables, focusing on variables reflecting drought severity such as VPD, and (iii) quantify the impacts of die-off event on forest resilience, measured considering the different response variables (vegetation indices, growth, GPP) to understand the changes in forest productivity after drought in die-off hotspots. We hypothesize that sites located in the driest sites (semi-arid biome) would show the highest responsiveness to drought in terms of canopy cover and greenness, growth and GPP reductions. We further propose that die-off sites could be used to diagnose forest responses to aridification.

2. Materials and Methods

2.1. Study Sites

This study encompasses 41 forest sites and 3 shrubland sites showing die-off events recorded in the field by our research team from the 1980s to the 2020s [26,27], located across Spain, and encompassing a wide range of climatic, geographic, and ecological conditions (Figure 1). We considered georeferenced sites with field observations of pulses of elevated tree mortality, high canopy defoliation (0%–30% dead trees or crown defoliation > 50% in more than 40% trees) and low growth rates in response to heat and drought stress affecting the dominant tree and shrub species across areas from ca. 0.5 to 2 ha [27]. We visited and sampled every site and determined the year of dieback onset when there was a continuous and abrupt drop in vegetation cover and greenness based on remote sensing data (see Section 2.3). In addition, we checked that the study sites were not affected by other disturbances such as wind storms or wildfires at least since 1970.

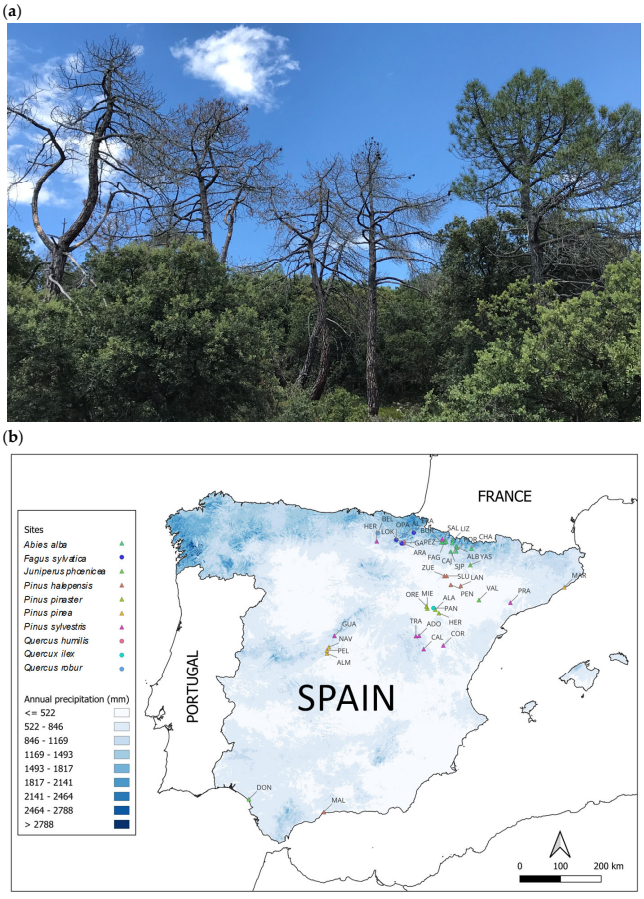

Figure 1. (**a**) View of a die-off hotspot (*Pinus pinaster* in Miedes de Aragón, site MIE). (**b**) Climate classification of the sites studied in Spain (see codes in Table 1). Different symbols show the studied species with triangles and circles indicating conifers and broadleaves, respectively. The background color scale shows annual precipitation across Spain.

Table 1. Characteristics of the study sites. VPD is the vapor pressure deficit.

Site (Code)	Main Species	Biome Type	Latitude (°N)	Longitude (°, −W, +E)	Elevation (m a.s.l.)	VPD (kPa)	Aridity Index	Dieback Years
Beluntza (BEL)	*Quercus robur*	Humid	42.950	−2.887	620	0.45	0.79	2017
Aramendia (ARA)	*Quercus humilis*	Humid	42.716	−2.111	675	0.48	0.82	2017
Alsasua (AL)	*Quercus robur*	Humid	42.897	−2.084	615	0.50	0.80	2016
Galdeano (GA)	*Quercus humilis*	Humid	42.735	−2.107	649	0.52	0.70	2017
Lokiz (LOK)	*Fagus sylvatica*	Humid	42.717	−2.170	989	0.51	0.72	2016
Eraso (ERA)	*Fagus sylvatica*	Humid	42.953	−1.801	547	0.49	0.82	2017
Opakua (OPA)	*Fagus sylvatica*	Humid	42.799	−2.331	1020	0.48	0.78	2005, 2012
Albarún (ALB)	*Abies alba*	Humid	42.606	−0.504	1470	0.56	0.70	1986, 2022
Castiello de Jaca (CAJ)	*Abies alba*	Humid	42.639	−0.534	1142	0.53	0.72	1986, 2022
Burgi (BUR)	*Abies alba*	Humid	42.727	−0.973	765	0.55	0.74	1986, 2022
Fago (FAG)	*Abies alba*	Humid	42.724	−0.882	957	0.54	0.70	1986, 2022
Salvatierra de Escá (SAL)	*Abies alba*	Humid	42.731	−0.916	827	0.54	0.72	1986, 2022
Chate (CHA)	*Abies alba*	Humid	42.570	−0.080	991	0.50	0.74	1986, 2022
Lopetón (LOP)	*Abies alba*	Humid	42.760	−0.850	1039	0.51	0.75	1986, 2022
Lizara (LIZ)	*Abies alba*	Humid	42.760	−0.630	1370	0.40	0.89	1986, 2022
Paco Ezpela (PEZ)	*Abies alba*	Humid	42.740	−0.830	1244	0.54	0.71	1986, 2022
Paco Mayor (PMA)	*Abies alba*	Humid	42.710	−0.650	1285	0.46	0.79	1986, 2022
Peña Oroel (POR)	*Abies alba*	Humid	42.520	−0.540	1733	0.53	0.69	1986, 2022
San Juan de la Peña (SJP)	*Abies alba*	Dry sub-humid	42.520	−0.700	991	0.58	0.63	1986, 2022
Roncal (RON)	*Pinus sylvestris*	Humid	42.802	−0.942	801	0.51	0.75	2012, 2022
Corbalán (COR)	*Pinus sylvestris*	Semi-arid	40.442	−0.988	1209	0.64	0.44	2012, 2022
Traid (TRA)	*Pinus sylvestris*	Dry sub-humid	40.661	−1.781	1457	0.65	0.52	2012, 2022
Prades (PRA)	*Pinus sylvestris*	Dry sub-humid	41.337	1.015	921	0.60	0.53	2012, 2022
Calomarde (CAL)	*Pinus sylvestris*	Humid	40.370	−1.56	1340	0.63	0.69	2012, 2022
Guadarrama (GUA)	*Pinus sylvestris*	Dry sub-humid	40.667	−4.155	1276	0.59	0.56	2012, 2022
Hereña (HER)	*Pinus sylvestris*	Dry sub-humid	42.770	−2.920	580	0.52	0.52	2012, 2022
Adobes (ADO)	*Pinus sylvestris*	Dry sub-humid	40.667	−1.687	1429	0.65	0.51	2012, 2022
Miedes de Aragón (MIE)	*Pinus pinaster*	Semi-arid	41.269	−1.434	986	0.73	0.37	2017
Orera (ORE)	*Pinus pinaster*	Semi-arid	41.317	−1.457	864	0.71	0.38	2017
Aladrén (ALA)	*Pinus pinaster*	Semi-arid	41.240	−1.195	1014	0.73	0.35	2020
Herrera de los Navarros (HER)	*Pinus pinaster*	Semi-arid	41.160	−1.096	947	0.69	0.38	2022
Arenys de Munt (MAR)	*Pinus pinea*	Dry sub-humid	41.612	2.624	98	0.60	0.60	2015, 2022
Almorox (ALM)	*Pinus pinea*	Semi-arid	40.275	−4.366	692	0.92	0.28	2015
Pelayos (PEL)	*Pinus pinea*	Semi-arid	40.340	−4.370	823	0.87	0.28	2015
Navas (NAV)	*Pinus pinea*	Semi-arid	40.414	−4.312	681	0.88	0.29	2019
Zuera (ZUE)	*Pinus halepensis*	Semi-arid	41.981	−0.909	571	0.77	0.36	2022
Lanaja (LAN)	*Pinus halepensis*	Semi-arid	41.753	−0.431	365	0.87	0.33	2022
Peñaflor (PEN)	*Pinus halepensis*	Semi-arid	41.781	−0.725	365	0.90	0.29	2022
Sierra de Luna (SLU)	*Pinus halepensis*	Semi-arid	41.980	−0.840	493	0.85	0.34	2022
Málaga (MAL)	*Pinus halepensis*	Semi-arid	36.725	−4.386	71	0.72	0.38	2022
Valcuerna (VAL)	*Juniperus phoenicea*	Semi-arid	41.425	0.093	136	0.90	0.31	2012
Yaso (YAS)	*Juniperus phoenicea*	Semi-arid	42.208	−0.126	717	0.81	0.44	2017
Doñana (DON)	*Juniperus phoenicea*	Semi-arid	36.967	−6.465	8	0.72	0.35	2005
Paniza (PAN)	*Quercus ilex*	Semi-arid	41.273	−1.249	810	0.77	0.33	2022

The sites spanned from humid temperate broadleaf forests in northern Spain dominated by broadleaves to mountain sub-humid pine forests in central and eastern Spain, and semi-arid Mediterranean pine and juniper shrublands (Doñana, Yaso, Valcuerna) in eastern and southern Spain, ensuring a wide gradient of environmental conditions (Table 1). In total, 11 species were studied, belonging to three major families of tree species in Europe (Pinaceae, Cupressaceae, and Fagaceae). The study stands were dominated by deciduous and evergreen broadleaves from temperate (*Quercus robur*, *Fagus sylvatica*) and Mediterranean (*Quercus ilex*) biomes, evergreen conifers from temperate and continental regions (*Abies alba*, *Pinus sylvestris*), and Mediterranean evergreen conifers from mid- to low-elevation drylands (*Pinus pinaster*, *Pinus pinea*, *Pinus halepensis*). In addition, Mediterranean evergreen conifer shrubs (*Juniperus phoenicea*) were also considered.

The main species of each site accounted for more than 60% of the total cover or basal area. All sites were considered natural stands, except five pine plantations sampled in Hereña, Aladrén, Herrera de los Navarros, Arenys de Munt, and Málaga. Soil conditions ranged from basic soils on marls or limestones in Pyrenean silver fir (*A. alba*) forests to acid, sandy soils in Doñana and Arenys de Munt coastal sites.

2.2. Climate Data

We used climate data from the Terraclimate dataset gridded at 4 km resolution because they provide homogeneous and quality-checked series [28]. This is a relatively homogeneous, well-replicated dataset which derives other variables using a simple water balance model. We extracted monthly climate variables including mean minimum (Tmin) and maximum (Tmax) temperatures, precipitation, soil moisture, climatic water deficit (Def; the difference between the reference and actual evapotranspiration), VPD, and the Palmer Drought Severity Index (PDSI) for the period 1980–2023 (Table S1).

As extreme droughts linked to die-off onset, we selected five years (1986, 1995, 2005, 2012, 2017) when at least 3 consecutive months should show mean PDSI values, calculated for all sites, lower than −4 (Figure S1). We excluded the 2022 drought because its PDSI values were not so low and not all sites have growth records until 2025.

Finally, the Aridity Index (AI) was computed for each site as the ratio between annual precipitation and potential evapotranspiration, i.e., the precipitation available in relation to atmospheric water demand [29]. The AI values were used to classify the study sites into three biome types (semi-arid, $0.20 < AI < 0.50$, $n = 17$ sites; dry sub humid, $0.50 < AI < 0.65$, $n = 7$ sites; and humid, $AI > 0.65$, $n = 21$ sites), allowing the comparison of responses to climate among biomes (Table 1). We acknowledge that this classification is unbalanced and that the study species and biomes are spatially clustered (e.g., humid sites in northern Spain; see Figure 1), but this was the intrinsic nature of the dataset which was also shaped by the regional extent of recent droughts.

2.3. Remote Sensing Data: Vegetation Indices and GPP

To analyze changes in canopy cover and greenness, we used two widely employed vegetation indices. The NDVI was calculated from the difference between the near-infrared (NIR) and red (R) reflectances [30]:

$$NDVI = \frac{NIR - (R)}{NIR + (R)} \quad (1)$$

The primary strengths of NDVI consist of its extensive spatial coverage and temporal resolution, which allow vegetation cover and greenness to be monitored across broad regions [24]. However, in the case of dense canopies, the NDVI shows saturation effects which have led to the use of the Enhanced Vegetation Index (EVI), which reduces the influence of atmospheric conditions through the use of the blue band, thus minimizing canopy saturation in dense vegetation of humid sites, although it may be sensitive to topographical influences [31–34]. The EVI was calculated with the following formula:

$$EVI = \frac{G \times (NIR - R)}{(NIR + C1 \times R - C2 \times B + L)} \quad (2)$$

where G is the gain factor (usually set to 2.5), $C1$ and $C2$ are the atmospheric resistance coefficients, L is an adjustment to correct for non-linear transmission of NIR and red radiation (R) through vegetation, and B is blue light [31].

Monthly NDVI and EVI data were downloaded from the https://landtrend.csic.es/ltr-vegchanges (accessed on 2 February 2026) platform [35], which is based on corrected and homogenized information from Landsat images [36–38]. These images were atmospherically corrected, a 30% cloud threshold was applied, and surface reflectivity values were harmonized between sensors of the Landsat image collection. We obtained annual and monthly NDVI and EVI values by calculating the medoid algorithm, a multidimensional analog of the median that selects the real pixel whose Euclidean distance is minimal from the median of all bands. The NDVI and EVI data were obtained by entering the coordinates

of each study site and considering a 90 m × 90 m area. The analyzed period covered 1984–2023 (Table S1). Raw and fitted annual NDVI and EVI values were obtained using linear regressions, which allowed calculating linear trends of NDVI and EVI (Table S1). Then, NDVI and EVI residuals (NDVIr and EVIr, respectively), representing year-to-year NDVI and EVI variability, were calculated as the differences between observed and fitted NDVI or EVI values.

For each site, monthly GPP was also obtained at 0.5º spatial resolution for the period 1979–2018 (Table S2) based on a dataset derived from remote sensing and eddy covariance flux tower data [39]. The GPP dataset was derived from satellite-derived (MODIS, 1 km resolution) solar-induced fluorescence and calibrated with GPP estimates from a subset of distributed eddy covariance flux towers. These data allowed the quantification of climate–GPP relationships and the GPP recovery dynamics after dieback. We selected three study cases representative of the three biome types to assess GPP changes before and after the dieback, considering a 3-year window. First, the 1985–1987 period and the Castiello de Jaca site were selected to represent mountain humid silver fir (*A. alba*) sites affected by the 1986 dieback event. Second, the 2011–2013 period was selected to represent Scots pine (*P. sylvestris*) dry sub-humid sites, and data corresponded to the Hereña site. Third, the 2016–2018 period was selected to represent semi-arid maritime pine (*P. pinaster*) sites, and data corresponded to the Miedes de Aragón site. For each site, monthly GPP anomalies were calculated with respect to the mean values of the period 1979–2018. Then, we tested whether monthly anomalies were significantly ($p < 0.05$) different from long-term monthly means using one-sample *t* tests.

2.4. Radial Growth

To assess radial growth trends and variability, we used tree-ring width data. At each site, between 15 and 80 dominant individuals of the main species (mean = 35 individuals per site) were cored at 1.3 m using a Pressler increment borer (Haglöf, Långsele, Sweden) following dendrochronological methods [40]. In the case of shrubs (Doñana site) and small trees (*Q. ilex* in Paniza), basal cross-sections were also obtained from 25 dying or dead individuals using a chainsaw. Wood cores or cross-sections were air-dried, mounted (only cores) and carefully sanded with sandpapers. Then, they were visually cross-dated under the binoculars. Samples were scanned at 2400 dpi resolution using a flatbed scanner (EPSON XL 10,000 scanner, Epson, Suwa, Japan) and two radii per individual were measured with a 0.001 mm resolution using the CooRecorder-CDendro software version 9.8.4 [41]. Cross-dating was checked using the COFECHA software, which calculates moving correlations between individual ring-width series and the mean site series [42].

To quantify growth trends, ring-width series were converted into basal area increment (BAI) series using the following formula:

$$BAI = \pi \times (R_t^2 - R_{t-1}^2) \quad (3)$$

where R_t is the stem radius at the end of the year t, and R_{t-1} is the stem radius at the end of the previous year. The BAI was calculated from the bark to the pith, assuming concentric growth (Table S1). The BAI represents the annual increase in basal area, providing a more accurate reflection of growth than ring-width measurements [43].

To characterize growth variability, ring-width values were transformed into ring-width indices (RWIs), which represent year-to-year growth variability and are used to calculate climate–growth relationships [40]. RWI individual series were calculated by first removing age-related and non-climatic trends from each ring-width series by fitting a 25-year smoothing spline. Then, RWIs were obtained by dividing observed values by fitted values, and the resulting indices were standardized. We removed most of their first-

order autocorrelation of ring-width indices by fitting autoregressive models and calculated sites' series of ring-width indices (chronologies) using bi-weight robust means [40]. To characterize each site chronology, we calculated the first-order autocorrelation of ring width (AR1) and the mean correlation between individual, indexed series (rbar), which measures the coherence of each site chronology (Table S1). All tree-ring calculations were done using the dplR package [44–46].

2.5. Resilience Indices

To assess post-drought canopy cover and growth recovery after severe droughts, resilience indices were calculated considering NDVI, NDVIr, EVI, EVIr, BAI, and RWI data [47]. This was done considering the selected dry years (1986, 1995, 2005, 2012 and 2017) and using a window of ±2 years, i.e., before and after the drought, given that most species show drought legacies lasting 1–2 years [8]. Resilience (*Rs*) was estimated by dividing the mean value of the variable two years following the drought year (PostDr) by the mean of the variable in the two previous years (PreDr):

$$Rs = \frac{PostDr}{PreDr} \quad (4)$$

2.6. Statistical Analyses

First, the Shapiro–Wilk test was used to evaluate the normality of considered variables. Most variables followed normality except precipitation, water deficit and BAI, which were log (x + 1) transformed. Second, linear regressions were computed for all climate variables against calendar year to quantify their trends. Third, Tukey's pairwise post hoc tests were calculated following ANOVA to compare variables (climate variables, BAI), trends and correlations (e.g., climate–NDVI or climate–BAI) between sites grouped as biome types. Lastly, Pearson correlation coefficients were used to calculate the relationships between monthly climate variables (Tmin, Tmax, precipitation, water deficit, soil moisture, VPD and PDSI), vegetation indices (NDVI, NDVIr, EVI, EVIr), growth metrics (BAI, RWI), and GPP. To assess climate–GPP relationships, we selected spring climate variables because they showed the stronger relationships. Correlations were also calculated between climate variables of the previous (t − 1) and current (t) years and response variables to detect lagged responses. The window of analyses spanned from prior September to current October. Analyses were done using the R statistical software version 4.5.3 [48].

3. Results

3.1. Climate Variability and Trends

Semi-arid sites showed the warmest conditions and highest VPD, followed by the dry sub-humid, and humid sites (Figure 2). Biomes showed significant differences regarding Tmin (F = 17.69, p = 0.0002), Tmax (F = 31.98, $p < 0.0001$), and VPD (F = 92.81, $p < 0.0001$). In all cases, semi-arid sites showed significantly warmer conditions (Tmin, p = 0.007; Tmax, p = 0.0001) and higher VPD (mean ± SD, 0.85 ± 0.08 kPa vs. 0.59 ± 0.03 kPa; p = 0.0001) than the other two biomes. Warming trends did not differ between biomes (Tmin, F = 3.52, p = 0.06; Tmax, F = 1.08, p = 0.36), but semi-arid sites showed higher VPD trends than the other biomes (0.0045 ± 0.0009 kPa year^{-1} vs. 0.0034 ± 0.0004 kPa year^{-1}; F = 19.14, p = 0.0001).

We also found significant differences in precipitation between biomes (F = 121.60, $p < 0.0001$). Humid sites showed a steeper precipitation trend than the other biomes (2.47 ± 0.81 mm year^{-1} vs. 0.51 ± 1.15 mm year^{-1}; F = 20.10, p = 0.0001), and higher soil moisture (F = 100.3, $p < 0.0001$). In contrast, semi-arid sites showed the highest water deficit (F = 268.0, $p < 0.0001$). All biomes showed similar negative trends regarding soil moisture (−0.11 ± 0.21 mm year^{-1}). The trends of water deficit were significantly higher

in semi-arid sites than in the other biomes (2.71 ± 0.61 mm year^{-1} vs. 1.89 ± 0.65 mm year^{-1}; $F = 10.50$, $p = 0.0015$). Lastly, humid sites showed significantly ($F = 79.34$, $p < 0.001$) lower annual PDSI values than the other biomes. Most sites showed negative PDSI trends with a mean value of −0.018 ± 0.0187 year^{-1}, but differences between biomes were not significant ($F = 0.41$, $p = 0.67$). In short, throughout the study period, climate showed a continuous warming trend, higher VPD and water deficit, particularly in semi-arid sites, leading to aridification.

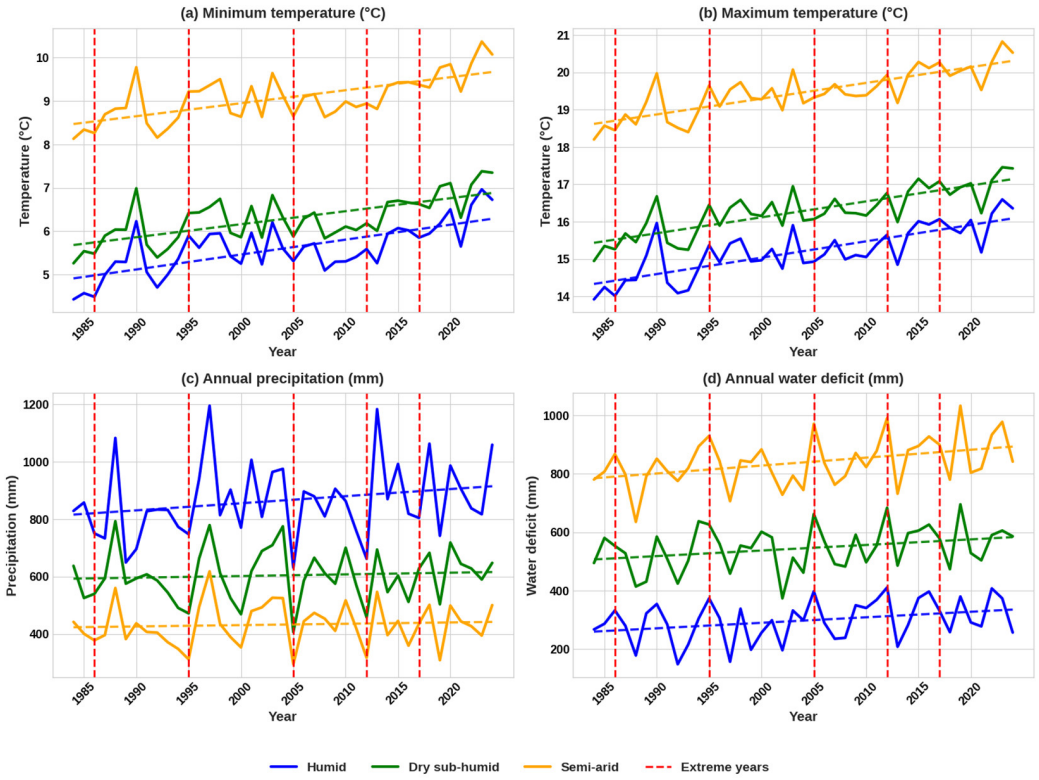

Figure 2. Annual climatic variables calculated for the three biomes (humid, dry sub-humid, and semi-arid sites) during 1984–2024. Panels show: (**a**) minimum temperature, (**b**) maximum temperature, (**c**) precipitation, and (**d**) water deficit (higher values indicate stronger deficit). Lines represent biome level means across all sites. Red dashed vertical lines mark the main droughts studied (1986, 1995, 2005, 2012, 2017).

3.2. Vegetation Indices

Humid sites showed higher annual NDVI ($F = 42.39$, $p < 0.001$; 0.74 ± 0.06 vs. 0.54 ± 0.08) and EVI ($F = 35.35$, $p < 0.001$; 2.02 ± 0.27 vs. 1.38 ± 0.27) values than the rest of the sites (Figure 3). No significant differences were found between biomes regarding NDVI ($F = 0.75$, $p = 0.49$; trend 0.0037 ± 0.001 year^{-1}) or EVI trends ($F = 1.05$, $p = 0.37$; trend 0.0032 ± 0.006 year^{-1}). No site showed a negative NDVI trend, whereas 31% of sites presented negative EVI trends and 57% of these sites were located in the humid biome. The mean annual series of NDVI showed significant ($p < 0.05$) and positive correlations ($r = 0.80$–0.91) between biomes, but this was not the case for EVI because humid and dry sub-humid sites showed a non-significant correlation, whilst dry sub-humid and semi-arid sites showed a stronger relationship ($r = 0.61$, $p < 0.001$; Figure 3). Again, the mean series of NDVI residuals (NDVIr) showed significant correlations between biomes ($r = 0.31$–0.53, $p < 0.05$), whereas only the series of EVI residuals (EVIr) of dry sub-humid and semi-arid sites showed a significant correlation ($r = 0.48$, $p = 0.002$).

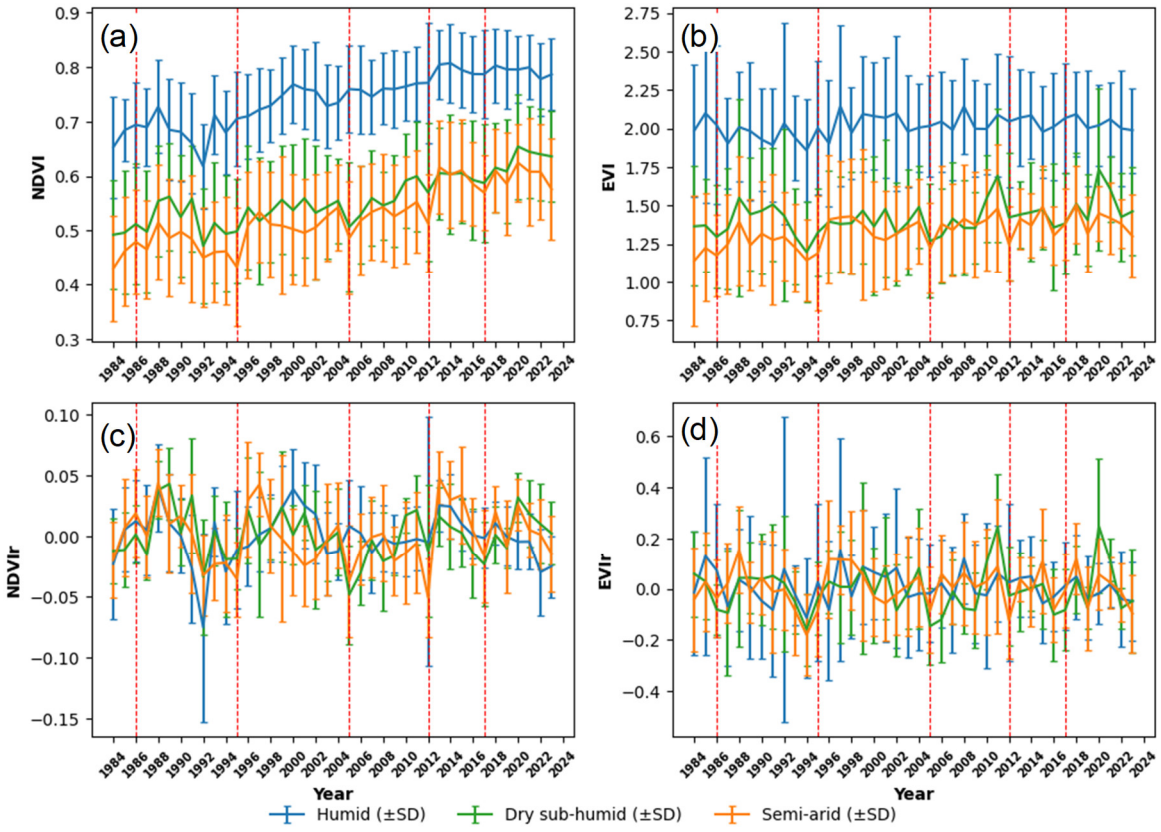

Figure 3. Temporal dynamics of vegetation indices ((**a**), NDVI, Normalized Difference Vegetation Index; (**b**) EVI, Enhanced Vegetation Index) and their residuals ((**c**), NDVIr; (**d**), EVIr) averaged by biome (humid, dry sub-humid, semi-arid). Lines represent biome level means, and error bars are standard deviations. The vertical red dashed lines represent major droughts.

3.3. Tree Radial Growth

Growth rates (BAI) were higher ($F = 6.31$, $p = 0.007$) in the humid sites (934 ± 714 mm^2) than in the sub-humid (577 ± 363 mm^2) and semi-arid (360 ± 279 mm^2) biomes (Figure 4). Regarding BAI trends, we found no significant differences between biomes ($F = 1.18$, $p = 0.33$; mean across sites = −3.35 ± 20.88 mm^2 year^{-1}), but a high variability between biomes and sites. We detected significant ($p < 0.001$) negative BAI trends in humid (−10.13 mm^2 year^{-1}) and dry sub-humid sites (−6.93 mm^2 year^{-1}), but semi-arid sites showed no significant BAI trend. The annual BAI series of all biomes showed significant correlations between them ($r = 0.49$–0.50, $p = 0.001$), except those from humid and semi-arid sites ($r = 0.21$, $p = 0.184$).

There were significant differences in growth indices (RWIs) between biomes ($F = 4.90$, $p = 0.019$), with dry sub-humid sites showing lower RWI values (0.979 ± 0.006) than semi-arid (0.989 ± 0.009) and humid sites (0.986 ± 0.008). The mean series of RWI in dry sub-humid and semi-arid biomes showed a significant positive correlation ($r = 0.68$, $p < 0.001$; Figure 4). Lastly, there were significant differences in RWI trends between biomes ($F = 3.48$, $p = 0.046$), with humid sites showing higher trends (0.00087 ± 0.0008 year^{-1}) than dry sub-humid (0.00054 ± 0.00110 year^{-1}) and semi-arid sites (0.00011 ± 0.00082 year^{-1}).

On average, the RWI and BAI during dry years were 77 ± 17% as compared with the rest of years, i.e., there was a relative growth reduction of −23% due to drought stress considering all sites and biomes (Figure 4). No significant difference was found when comparing the relative RWI and BAI reductions during drought years ($F = 2.92$, $p = 0.12$; and $F = 3.55$, $p = 0.08$, respectively).

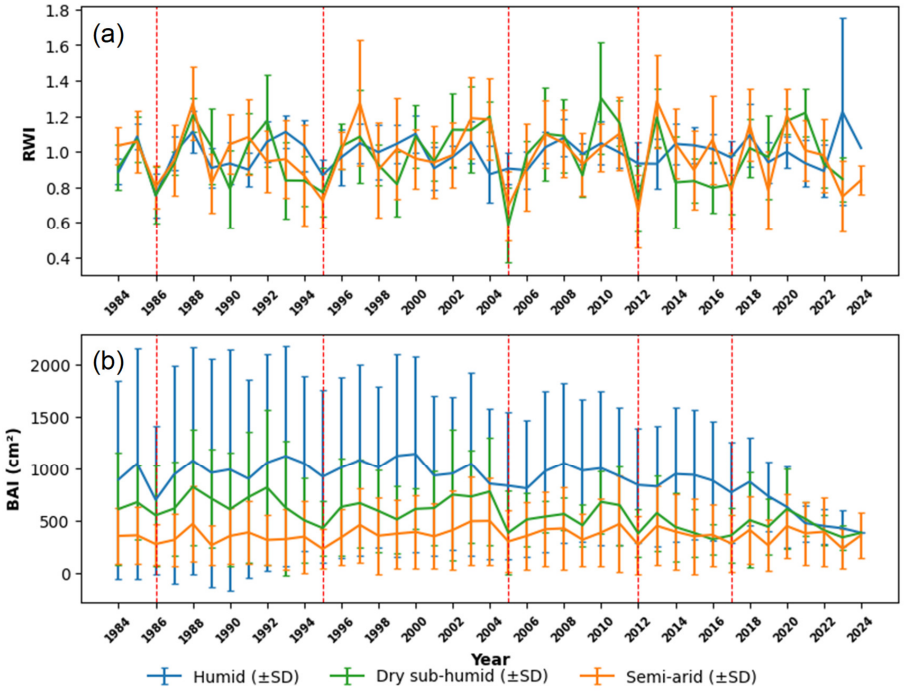

Figure 4. Temporal patterns of tree growth metrics ((**a**), RWI, ring-width index; (**b**), BAI, basal area increment) shown for humid, dry sub-humid, and semi-arid sites. Lines represent biome level averages, and error bars are standard deviations. The vertical dashed lines represent major droughts.

3.4. Relationships Between Canopy Activity and Growth

The correlations between annual values of NDVI or EVI and BAI peaked in semi-arid sites, being significantly higher than in humid sites (NDVI-BAI, $F = 4.12$, $p = 0.031$; EVI-BAI, $F = 5.31$, $p = 0.016$; Figure 5). A similar result was found for the correlations between NDVIr and RWI ($F = 11.94$, $p = 0.0007$), whereas the correlations between EWIr and RWI peaked again in semi-arid sites ($F = 12.13$, $p = 0.0006$).

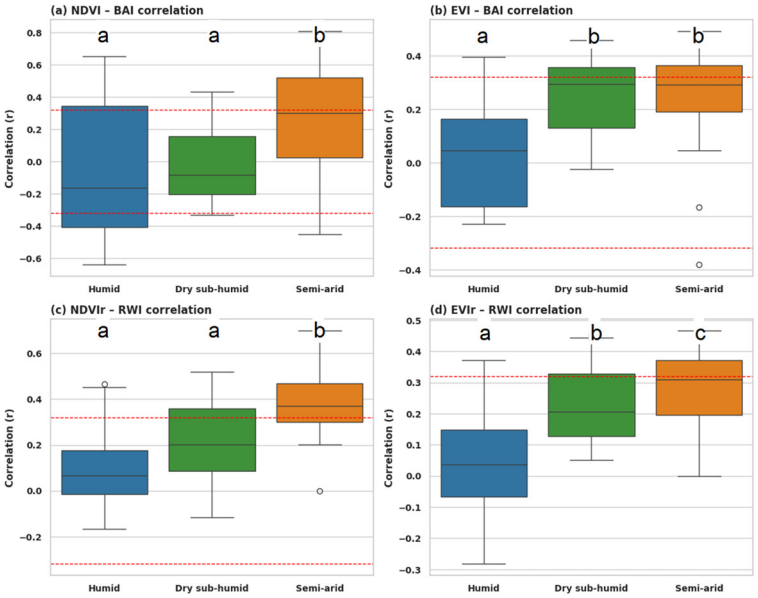

Figure 5. Boxplot comparisons of correlations between canopy activity metrics (NDVI, Normalized Difference Vegetation Index; EVI, Enhanced Vegetation Index; NDVIr, NDVI residuals; EVIr, EVI residuals) and tree growth metrics (BAI, basal area increment; RWI, ring-width index) across biomes: (**a**) NDVI-BAI, (**b**) EVI-BAI, (**c**) NDVIr-RWI, and (**d**) EVIr-RWI. The horizontal dashed lines show the 0.05 significance levels. Different letters indicate significant ($p < 0.05$) differences between sites.

3.5. Climate Drivers of Canopy Activity and Growth

Most significant ($p < 0.05$) correlations between monthly climate variables and the corresponding canopy and growth metrics were positive. They peaked in the case of PDSI and RWI or BAI, indicating that growth was the most sensitive variable to drought severity (Figure 6). This was followed by the VPD-NDVI and Tmax-NDVI positive correlations, which are due to the long-term increase in both temperature and NDVI since NDVIr did not show these relationships. Both NDVI and EVIr responded positively to PDSI and soil moisture. BAI also responded positively to PDSI, but negatively to VPD and temperature in some sites, indicating sensitivity to atmospheric water demand. In general, RWI decreased as the water deficit increased.

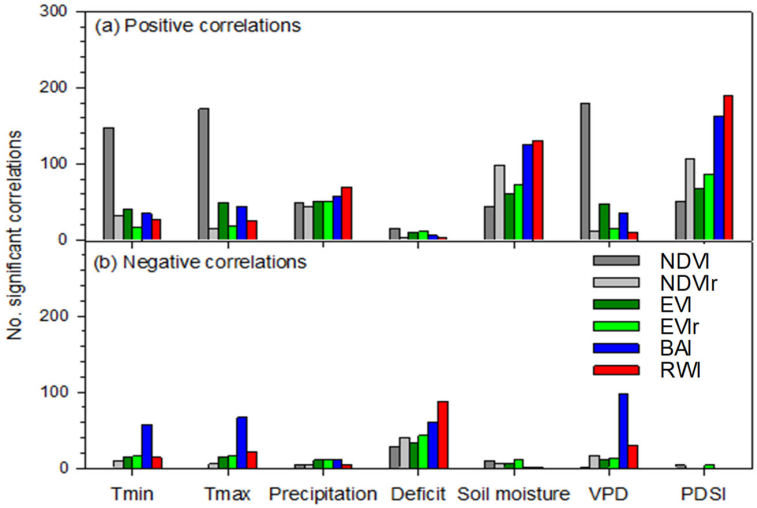

Figure 6. (**a**) Positive and (**b**) negative significant ($p < 0.05$) correlations obtained by relating monthly climate variables and vegetation (NDVI, Normalized Difference Vegetation Index; EVI, Enhanced Vegetation Index; NDVIr, NDVI residuals; EVIr, EVI residuals) or tree growth metrics (BAI, basal area increment; RWI, ring-width index).

In the case of the significant positive correlations between PDSI and BAI or RWI, 16%, 23% and 61% of them corresponded to humid, dry sub-humid and semi-arid sites, respectively. As expected, the number of significant positive correlations between PDSI and RWI or NDVIr peaked in the driest semi-arid sites. When focusing on the most important relationships, we found that 47% of the positive and significant correlations between VPD and NDVI were found in semi-arid sites (Figure S2). Indeed, the number of significant positive correlations between PDSI and RWI or NDVIr showed significant negative correlations with the site Aridity Index (RWI, Spearman $r_s = -0.71$; NDVIr, $r_s = -0.55$, $p < 0.001$ in both cases), i.e., the sensitivity to drought increased as site aridity did.

3.6. Climate–GPP Relationships

The mean GPP values ranged considerably (1.25–3.66 g C m^{-2} d^{-1}), showing a mean value of 2.50 g C m^{-2} d^{-1} (period 1979–2018; Table S2). The three biomes showed significantly different mean GPP values ($F = 137$, $p < 0.001$) with mean values of 3.39, 2.21 and 1.57 g C m^{-2} d^{-1} for humid, dry sub-humid and semi-arid sites, respectively.

Warmer conditions enhanced annual GPP in humid sites, whereas elevated water deficit and drought (low precipitation and soil moisture, low PDSI values) constrained GPP in dry sub-humid and semi-arid sites, but not in humid sites (Figure 7). The GPP of humid sites was more responsive to minimum ($F = 33.87$) and maximum temperatures ($F = 37.99$), and to precipitation ($F = 376.10$), water deficit ($F = 100.40$), soil moisture ($F = 69.60$), VPD ($F = 7.19$), and PDSI ($F = 275.90$) than the other two biomes ($p < 0.01$ in all cases).

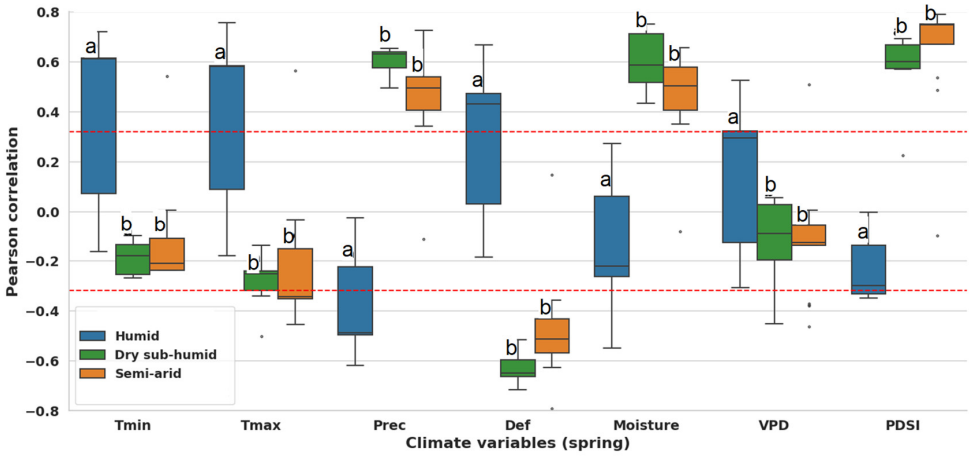

Figure 7. Pearson correlations calculated between gross primary productivity (GPP) and spring climate variables for the three biome types. Horizontal dashed lines show 0.05 significance levels. Different letters indicate significant ($p < 0.05$) differences between sites.

3.7. GPP Anomalies During Dieback Episodes

On average, the GPP during dry years was 95.6 ± 4.1% as compared with the rest of the years, i.e., there was a relative GPP reduction of −4.4% due to drought. There were significant differences in drought-related GPP reduction between biomes ($F = 34.15$, $p < 0.001$), with dry sub-humid and semi-arid sites showing stronger GPP decreases (−5.3 ± 0.8% and −6.8 ± 0.9%, respectively) than humid sites (−1.4 ± 0.3%).

In relative terms, drought-induced negative monthly GPP anomalies during years of die-off onset were similar among sites. Significant negative GPP anomalies (ca. −50% reductions) were found during spring and summer months of the die-off years in the three biomes (Figures 8–10). No post-dieback significant negative anomaly (legacy effect) was found one year after the die-off.

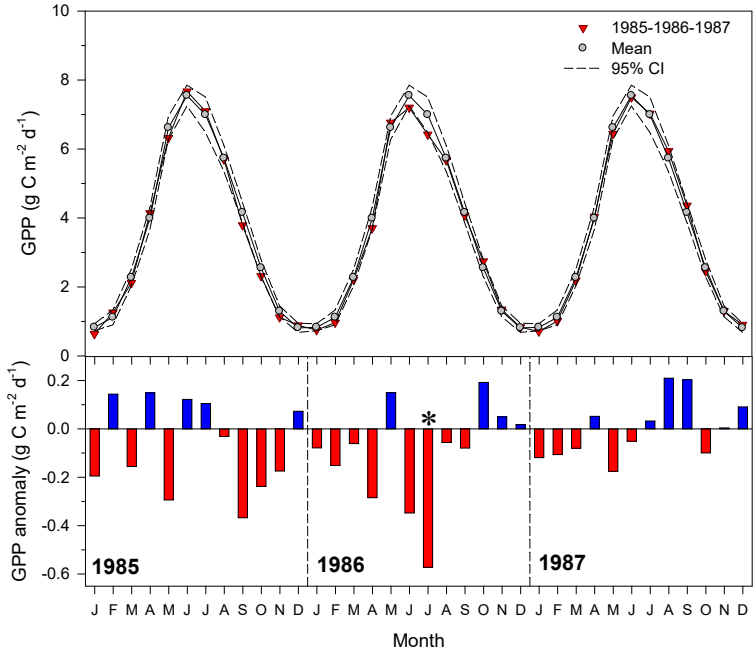

Figure 8. Monthly gross primary productivity (GPP) values from 1985 to 1987 in a humid silver fir site (Castiello de Jaca) and GPP anomalies (bars). In the upper plot, the lines show the means ± 95 confidence intervals, and the red symbols show the monthly values for the period 1985–1987. In the lower plot, red and blue bars indicate negative and positive GPP anomalies, respectively. Asterisks indicate values significantly ($p < 0.05$) different from the corresponding monthly means.

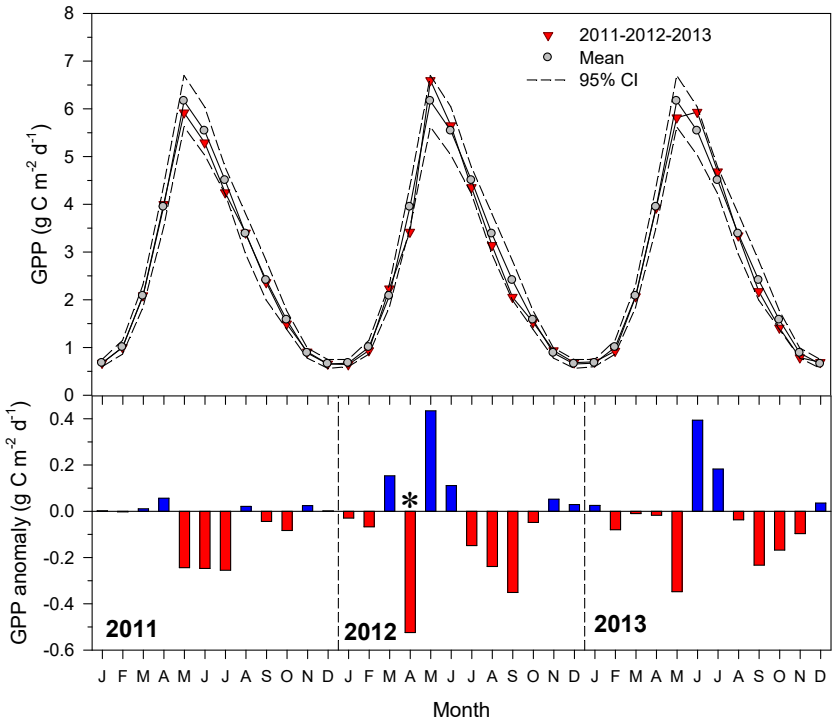

Figure 9. Monthly gross primary productivity (GPP) values from 2011 to 2012 in a dry sub-humid Scots pine site (Hereña) and GPP anomalies (bars). In the upper plot, the lines show the means ± 95 confidence intervals, and the red symbols show the monthly values for the period 2011–2013. In the lower plot, red and blue bars indicate negative and positive GPP anomalies, respectively. Asterisks indicate values significantly ($p < 0.05$) different from the corresponding monthly means.

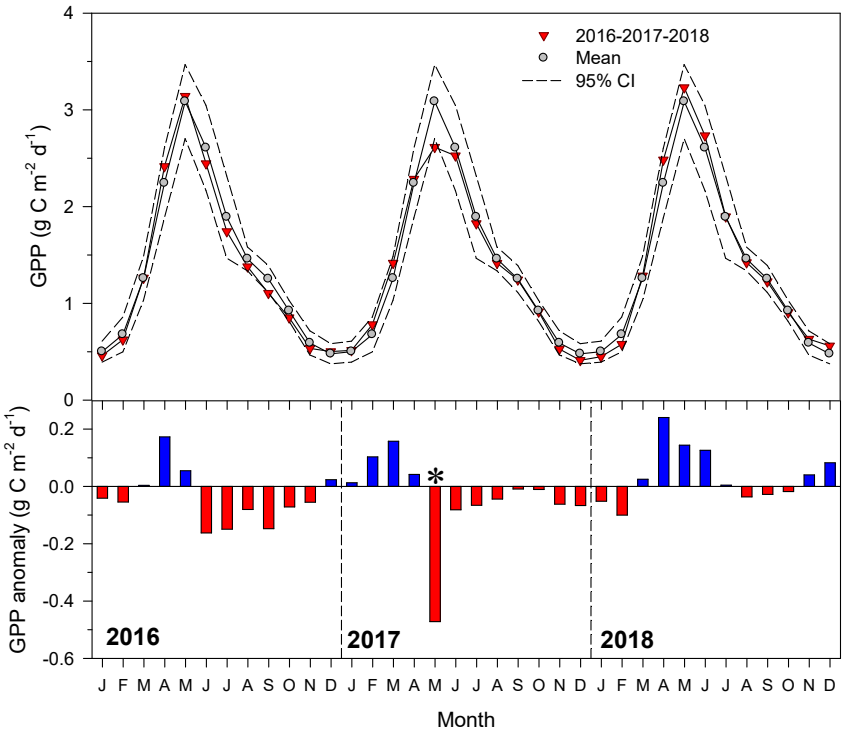

Figure 10. Monthly gross primary productivity (GPP) values from 2016 to 2018 in a semi-arid maritime pine site (Miedes de Aragón) and GPP anomalies (bars). In the upper plot, the lines show the means ± 95 confidence intervals, and the red symbols show the monthly values for the period 2016–2018. In the lower plot, red and blue bars indicate negative and positive GPP anomalies, respectively. Asterisks indicate values significantly ($p < 0.05$) different from the corresponding monthly means.

3.8. Drought Resilience

The resilience indices calculated for selected droughts and using either vegetation indices (NDVI, EVI) or growth metrics (BAI, RWI) did not significantly differ between biomes (Table 2). However, semi-arid sites showed a significantly higher GPP resilience than the other two biomes.

Table 2. Resilience values (means ± SD) calculated for annual values of the vegetation indices (NDVI, Normalized Difference Vegetation Index; EVI, Enhanced Vegetation Index;), growth metrics (BAI, basal area increment; RWI, ring-width index), and gross primary productivity (GPP). The last line shows the statistics (F, p) of ANOVAs comparing different biomes. Different letters indicate significant ($p < 0.05$) differences between biomes.

Biome	NDVI	EVI	BAI	RWI	GPP
Humid	1.04 ± 0.03	1.01 ± 0.02	0.97 ± 0.08	1.00 ± 0.04	1.01 ± 0.01 a
Dry sub-humid	1.05 ± 0.04	1.03 ± 0.06	1.05 ± 0.25	1.06 ± 0.17	1.01 ± 0.01 a
Semi-arid	1.08 ± 0.07	1.08 ± 0.07	1.07 ± 0.14	1.04 ± 0.10	1.06 ± 0.01 b
F	0.87	1.76	1.05	0.66	322
p	0.46	0.25	0.40	0.55	0.001

The resilience indices did not differ when comparing the different response variables (NDVI, EVI, BAI, RWI, GPP) regardless of the biome type ($F = 0.42$, $p = 0.74$). However, there were significantly different resilience values between the five droughts compared ($F = 6.11$, $p = 0.0012$). Specifically, the resilience values of 1995 were significantly higher (1.11 ± 0.09) than those of 2005 (0.97 ± 0.06) and 2012 (1.00 ± 0.08) (Figure 11).

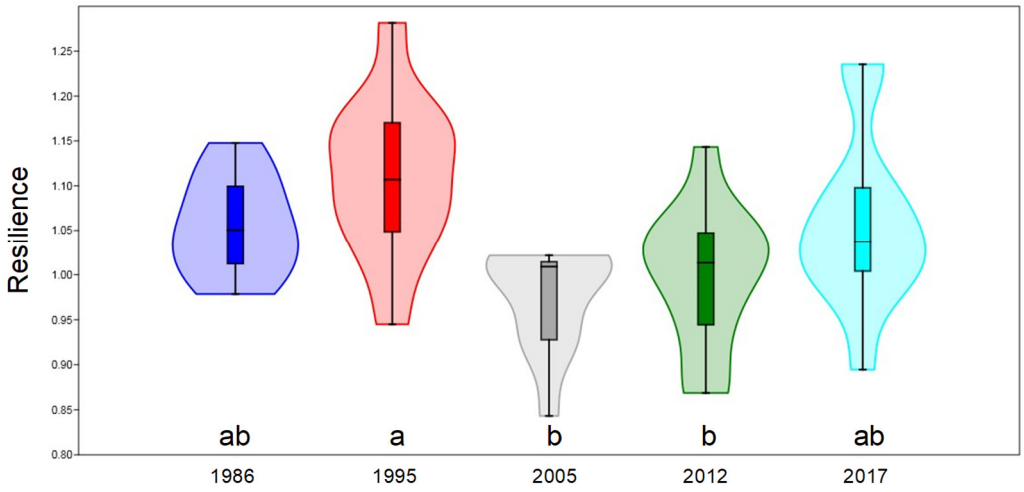

Figure 11. Violin and boxplots showing resilience values obtained for the main response variables (NDVI, Normalized Difference Vegetation Index; EVI, Enhanced Vegetation Index; BAI, basal area increment; RWI, ring-width index; GPP, gross primary productivity) considering the five selected droughts (1986, 1995, 2005, 2012, 2017). Different letters indicate significant ($p < 0.05$) differences between years.

4. Discussion

We found distinct couplings and responses to climate of vegetation indices, growth metrics and GPP in drought die-off forests and shrublands. Drought stress reduced canopy cover and greenness, growth and GPP in both broadleaves and conifers, but responses were amplified by site aridity.

4.1. Aridification Strengthens Canopy–Growth Coupling and Their Responses to Drought

Climate warming has risen VPD and reduced soil moisture in the study sites since the 1980s, leading to aridification and making dry sub-humid and semi-arid sites prone

to die-off and growth decline. In contrast, humid sites showed notable growth and GPP reductions in response to rare, hotter droughts such as Pyrenean silver fir stands during 1986 [49]. Such compound climate events [6], characterized by elevated summer VPD and dry soils, seem to be responsible for the die-off affecting humid conifer forests [50,51].

Interestingly, the mean BAI series of all sites are converging, regardless of biome type, which indicates a long-term loss in productivity not captured by remote-sensing studies focusing on broad-scale greening rather than on local browning [12]. Tree growth decreased during dry years, and vegetation and growth indices were strongly coupled in semi-arid sites as expected. This explains why NDVI residuals and growth indices, reflecting year-to-year variability in canopy cover and greenness and wood production, were more responsive to drought severity as site aridity increased.

Vegetation indices showed the largest declines during extreme droughts in dry sub-humid and semi-arid sites, a pattern already reported at local to continental scales [52]. Under humid conditions, the phenology of primary and secondary growth may be less coupled through time than in drier sites, leading to less consistent relationships between canopy cover or greenness and radial growth. Nevertheless, matching the spatial and temporal scales of satellite-derived information with field data (growth, defoliation, mortality) remains a challenging issue [53]. In general, heat stress and elevated VPD seem to be the triggers of most of the studied die-off events characterized by exceptional drops in EVI and radial growth [17,50].

4.2. Rapid and Robust Post-Drought Recovery

During some drought events (e.g., 1986, 1995), growth reduction was modest and close to 20% (Figure 4), which may not express the full resistance and resilience capacity of the forests studied. In contrast, the 2005 drought event was the most severe (Figure 11), reduced growth by up to 40% in dry sub-humid and semi-arid sites, and better reflected post-drought resilience dynamics. Specifically, the 1986 event was abrupt and recovery took 1–2 years with growth surpassing pre-drought levels two years later. The 1995 event developed for two years and recovery required nearly two years to return to previous growth levels. The 2005 event was abrupt and recovery also required nearly two years, showing an evident hysteresis effect since growth did not recover to pre-drought levels. The 2012 event was abrupt and also triggered a strong growth reduction (ca. 40%) in dry sub-humid and semi-arid sites, but recovery to pre-disturbance levels was fast, taking one year. In this drought, humid sites showed little or no change. Lastly, the 2017 event occurred after approximately three years of relative stability and reduced growth by up to 30%, mainly in semi-arid sites, and recovery occurred within one year.

The recovery of vegetation and growth indices occurred within two years after drought, whereas GPP showed the highest resilience in semi-arid sites. This agrees with the lack of legacy effects reported in other tree-ring and GPP studies [25], confirming that spring–summer negative GPP anomalies observed during die-off years in the three biomes were compensated thereafter. Regarding radial growth, the post-stress rebound effect [54], more frequent in conifers than in broadleaves, may compensate for stronger negative legacies due to drought. Overall, resilience indices greater than one should be interpreted with caution because they can be caused by favorable climatic conditions after the disturbance year, boosting post-drought canopy activity, growth or GPP. Therefore, our analyses could be refined by incorporating climate conditions before and after the considered droughts into individual-based, mixed-effects growth models. For instance, exceptionally wet conditions have been shown to compensate for growth reductions caused by drought in semi-arid conifer forests [55].

In general, the obtained GPP reduction (−4.4%) due to drought is within the range (−13.4 to −3.2%) reported recently [56]. In addition, dry sub-humid and semi-arid sites showed the strongest GPP reductions and were those prone to present local legacy effects, as evidenced by this study and the mentioned global assessment [56]. This is supported by the highest GPP sensitivity to spring temperature and moisture in seasonally dry biomes. In the future, we aim to test whether growth and growing-season GPP are more coupled in dry sub-humid and semi-arid forests than in humid sites, and consider additional predictors of growth such as basal area and soil nitrogen availability.

4.3. Limitations of the Study

Finally, three caveats or limitations of our approach must be discussed. First, NDVI and EVI signals may also include signals from the understory and soil, particularly in the driest shrubland sites, which showed the lowest cover values. In addition, stand structure (e.g., pure vs. mixed stands, natural vs. planted forests) and leaf habit (evergreen vs. deciduous species) of the dominant tree and shrub species could affect NDVI and EVI variability and trends. Second, the mismatch between response variables may be explained by the different spatial and temporal resolutions of climate, remote sensing and tree-ring data. Third, our study sites were spatially clustered, thus sharing comparable climate conditions and gridded GPP data between neighboring sites, which may affect the significance levels of the statistical analyses. For this reason, we opted for presenting the GPP analyses for different biomes. The location of sites could explain the stronger EVI-RWI relationships between dry sub-humid and semi-arid sites, which would respond to similar atmospheric circulation patterns. The resolution of the derived GPP data may be too coarse for small-scale die-off sites, adding additional uncertainty and warranting the use of more finely resolved GPP data in future analyses.

5. Conclusions

By using die-off forests and shrublands as diagnostic monitoring sites, we evidenced that vegetation indices, growth and GPP decreased due to drought stress and recovered afterwards. Radial growth variability was the variable most responsive to soil drought, represented by a drought index, whereas NDVI was the most responsive to atmospheric drought, measured as VPD. The strongest coupling between vegetation indices, particularly EVI, and growth occurred in semi-arid sites, whereas GPP responded more positively to cool, moist spring conditions in humid sites. Semi-arid sites responded strongly to water deficit, but also presented the highest GPP resilience. Our results reconcile widespread long-term broad-scale greening and the expansion of forests and shrublands with localized browning and vegetation die-off. The resilience observed at the affected die-off sites is notable, but continued on-ground monitoring is needed to determine whether survival thresholds are exceeded, potentially triggering irreversible shifts (e.g., from forest to shrubland or from shrubland to steppe).

Supplementary Materials: The following supporting information can be downloaded at https://www.mdpi.com/article/10.3390/f17060710/s1. Figure S1: Selection of drought years (1986, 1995, 2005, 2012, 2017). The points show the mean monthly PDSI values calculated for all the study sites (error bars are SD). The red vertical lines show consecutive PDSI values lower than −4. The dashed horizontal line shows the selected threshold (PDSI = −4); Figure S2: Positive and negative significant ($p < 0.05$) correlations obtained by relating monthly climate variables and vegetation (NDVI, NDVIr, EVI, EVIr) or growth metrics (BAI, RWI) grouped by biomes; Table S1: Climate characteristics (annual values), vegetation indices (NDVI, EVI), and growth metrics (BAI, AR1, rbar) of the study sites. Trends of vegetation indices and BAI are calculated as linear slopes for the common period 1984–2023. Bold values indicate significant BAI slopes ($p < 0.05$); Table S2: GPP values estimated for each study

site. Values are means ± SD calculated for the period 1979–2018. Note that several sites located in the same grid share the same GPP values.

Author Contributions: Conceptualization, A.P., J.J.C. and A.G.; methodology, A.P., C.V., M.C., M.P., A.G. and E.G.d.A.; software, A.P., C.V., M.P. and J.J.C.; validation, A.P., C.V., J.L., M.P. and J.J.C.; formal analysis, A.P., C.V., M.P. and J.J.C.; investigation, A.P., M.C., X.L., J.L., J.J.C. and A.G.; resources, A.P., M.C., J.L., J.J.C. and A.G.; data curation, A.P., M.P., C.V., X.L., E.G.d.A. and J.J.C.; writing—, A.P. and J.J.C.; writing—review and editing, A.P., J.J.C., C.V., M.C., J.L., X.L., M.P., E.G.d.A. and A.G.; visualization, A.P., M.P. and J.J.C.; supervision, A.G. and J.J.C.; project administration, A.G., E.G.d.A. and J.J.C.; funding acquisition, A.G. and J.J.C. All authors have read and agreed to the published version of the manuscript.

Funding: This research was funded by "Ministerio de Ciencia e Invonvación" (Spain), grant numbers PID2021-123675OB-C43 and TED2021-129770B-C21. AP acknowledges funding through a CIHEAM-IAMZ master scholarship. CV and EGA were supported by the Johannes Amos Comenius Programme (P JAC), project No. CZ.02.01.01/00/22_008/0004605, Natural and anthropogenic georisks.

Data Availability Statement: Data are available on reasonable request to the corresponding author.

Acknowledgments: We thank several colleagues for or helping in the sampling of the study sites.

Conflicts of Interest: The authors declare no conflicts of interest.

References

1. IPCC. Summary for Policymakers. In *Climate Change 2023: Synthesis Report*; Lee, H., Romero, J., Eds.; IPCC: Geneva, Switzerland, 2003; pp. 1–34. [CrossRef]
2. Cook, B.I.; Mankin, J.S.; Marvel, K.; Williams, A.P.; Smerdon, J.E.; Anchukaitis, K.J. Twenty-First Century Drought Projections in the CMIP6 Forcing Scenarios. *Earth's Future* **2020**, *8*, e2019EF001461. [CrossRef]
3. Breshears, D.D.; Cobb, N.S.; Rich, P.M.; Price, K.P.; Allen, C.D.; Balice, R.G.; Romme, W.H.; Kastens, J.H.; Floyd, M.L.; Belnap, J.; et al. Regional vegetation die-off in response to global-change-type drought. *Proc. Natl. Acad. Sci. USA* **2005**, *102*, 15144–15148. [CrossRef]
4. Allen, C.D.; Breshears, D.D.; McDowell, N.G. On Underestimation of Global Vulnerability to Tree Mortality and Forest Die-off from Hotter Drought in the Anthropocene. *Ecosphere* **2015**, *6*, 1–55. [CrossRef]
5. Hammond, W.M.; Williams, A.P.; Abatzoglou, J.T.; Adams, H.D.; Klein, T.; López, R.; Sáenz-Romero, C.; Hartmann, H.; Breshears, D.D.; Allen, C.D. Global field observations of tree die-off reveal hotter-drought fingerprint for Earth's forests. *Nat. Comm.* **2022**, *13*, 1761. [CrossRef]
6. Gazol, A.; Camarero, J.J. Compound Climate Events Increase Tree Drought Mortality across European Forests. *Sci. Total Environ.* **2022**, *816*, 151604. [CrossRef]
7. Lazoglou, G.; Hadjinicolaou, P.; Sofokleous, I.; Bruggeman, A.; Zittis, G. Climate Change and Extremes in the Mediterranean Island of Cyprus: From Historical Trends to Future Projections. *Environ. Res. Commun.* **2024**, *6*, 095020. [CrossRef]
8. Gazol, A.; Camarero, J.J.; Vicente-Serrano, S.M.; Sánchez-Salguero, R.; Gutiérrez, E.; de Luis, M.; Sangüesa-Barreda, G.; Novak, K.; Rozas, V.; Tíscar, P.A.; et al. Forest resilience to drought varies across biomes. *Glob. Change Biol.* **2018**, *24*, 2143–2158. [CrossRef]
9. Valeriano, C.; Gazol, A.; Colangelo, M.; Camarero, J.J. Drought drives growth and mortality rates in three pine species under Mediterranean conditions. *Forests* **2022**, *12*, 1700. [CrossRef]
10. Camarero, J.J.; Gazol, A.; Sangüesa-Barreda, G.; Oliva, J.; Vicente-Serrano, S.M. To die or not to die: Early-warning signals of dieback in response to a severe drought. *J. Ecol.* **2015**, *103*, 44–57. [CrossRef]
11. Gazol, A.; Camarero, J.J.; Sangüesa-Barreda, G.; Vicente-Serrano, S.M. Post-drought Resilience After Forest Die-Off: Shifts in Regeneration, Composition, Growth and Productivity. *Front. Plant Sci.* **2018**, *9*, 1546. [CrossRef] [PubMed]
12. Khoury, S.; Coomes, D.A. Resilience of Spanish Forests to Recent Droughts and Climate Change. *Glob. Change Biol.* **2020**, *26*, 7079–7098. [CrossRef]
13. Yan, Y.; Piao, S.; Hammond, W.M.; Chen, A.; Hong, S.; Xu, H.; Munson, S.M.; Myneni, R.B.; Allen, C.D. Climate-Induced Tree-Mortality Pulses Are Obscured by Broad-Scale and Long-Term Greening. *Nat. Ecol. Evol.* **2024**, *8*, 912–923. [CrossRef]
14. Lausch, A.; Erasmi, S.; King, D.; Magdon, P.; Heurich, M. Understanding Forest Health with Remote Sensing -Part I—A Review of Spectral Traits, Processes and Remote-Sensing Characteristics. *Remote Sens.* **2016**, *8*, 1029. [CrossRef]
15. Torres, P.; Rodes-Blanco, M.; Viana-Soto, A.; Nieto, H.; García, M. The Role of Remote Sensing for the Assessment and Monitoring of Forest Health: A Systematic Evidence Synthesis. *Forests* **2021**, *12*, 1134. [CrossRef]

16. Rogers, B.M.; Solvik, K.; Hogg, E.H.; Ju, J.; Masek, J.G.; Michaelian, M.; Berner, L.T.; Goetz, S.J. Detecting Early Warning Signals of Tree Mortality in Boreal North America Using Multiscale Satellite Data. *Glob. Change Biol.* **2018**, *24*, 2284–2304. [CrossRef] [PubMed]
17. Crespo-Antia, J.P.; Gazol, A.; Pizarro, M.; González de Andrés, E.; Valeriano, C.; Cuadrado, Á.R.; Linares, J.C.; Camarero, J.J. Matching Vegetation Indices and Tree Vigor in Pyrenean Silver Fir Stands. *Remote Sens.* **2024**, *16*, 4564. [CrossRef]
18. Wang, Z.; Lyu, L.; Liu, W.; Liang, H.; Huang, J.; Zhang, Q.-B. Topographic Patterns of Forest Decline as Detected from Tree Rings and NDVI. *Catena* **2021**, *198*, 105011. [CrossRef]
19. Bunn, A.G.; Hughes, M.K.; Kirdyanov, A.V.; Losleben, M.; Shishov, V.V.; Berner, L.T.; Oltchev, A.; Vaganov, E.A. Comparing Forest Measurements from Tree Rings and a Space-Based Index of Vegetation Activity in Siberia. *Environ. Res. Lett.* **2013**, *8*, 035034. [CrossRef]
20. Vicente-Serrano, S.M.; Camarero, J.J.; Olano, J.M.; Martín-Hernández, N.; Peña-Gallardo, M.; Tomás-Burguera, M.; Gazol, A.; Azorin-Molina, C.; Bhuyan, U.; El Kenawy, A. Diverse Relationships between Forest Growth and the Normalized Difference Vegetation Index at a Global Scale. *Remote Sens. Environ.* **2016**, *187*, 14–29. [CrossRef]
21. Zhang, T.; Song, J.; Fan, Y.; Liu, Y.; Yu, S.; Guo, D.; Hou, T.; Guo, K. Vegetation Index Research on the Basis of Tree-Ring Data: Current Status and Prospects. *Forests* **2023**, *14*, 2016. [CrossRef]
22. Wei, M.; Jiao, L.; Zhang, P.; Wu, X.; Xue, R.; Du, D. Spatio-Temporal Diversity in the Link between Tree Radial Growth and Remote Sensing Vegetation Index of Qinghai Spruce on the Northeastern Margin of the Tibetan Plateau. *Forests* **2023**, *14*, 260. [CrossRef]
23. Gallardo, V.B.; Hadad, M.A.; Roig, F.A.; Gatica, G.; Chen, F. Spatio-Temporal Linkage Variations between NDVI and Tree Rings on the Leeward Side of the Northern Patagonian Andes. *For. Ecol. Manag.* **2024**, *553*, 121593. [CrossRef]
24. Leduc, F.; Coops, N.C.; Morin-Bernard, A.; Moreau, G.; Achim, A. A Review of Dendrochronology and Remote Sensing Integration for Forest Growth and Disturbance Monitoring. *Curr. For. Rep.* **2025**, *11*, 25. [CrossRef] [PubMed]
25. Yang, L.; Anderegg, W.R.L. Climate-driven tree mortality alters the timing and magnitude of forest carbon uptake in the conterminous United States. *Geophys. Res. Lett.* **2026**, *53*, e2025GL120746. [CrossRef]
26. Camarero, J.J.; Bigler, C.; Linares, J.C.; Gil-Pelegrín, E. Synergistic Effects of Past Historical Logging and Drought on the Decline of Pyrenean Silver Fir Forests. *For. Ecol. Manag.* **2011**, *262*, 759–769. [CrossRef]
27. Gazol, A.; Pizarro, M.; Hammond, W.H.; Allen, C.D.; Camarero, J.J. Droughts preceding tree mortality events have increased in duration and intensity, especially in dry biomes. *Nat. Comm.* **2025**, *16*, 5779. [CrossRef]
28. Abatzoglou, J.T.; Dobrowski, S.Z.; Parks, S.A.; Hegewisch, K.C. TerraClimate, a High-Resolution Global Dataset of Monthly Climate and Climatic Water Balance from 1958–2015. *Sci. Data* **2018**, *5*, 170191. [CrossRef]
29. Zomer, R.J.; Xu, J.; Trabucco, A. Version 3 of the Global Aridity Index and Potential Evapotranspiration Database. *Sci. Data* **2022**, *9*, 409. [CrossRef]
30. Rouse, J.W.; Haas, R.H.; Schell, J.A.; Deering, D.W. Monitoring Vegetation Systems in the Great Plains with ERTS. *NASA Spec. Publ.* **1974**, *1*, 309.
31. Huete, A. A Comparison of Vegetation Indices over a Global Set of TM Images for EOS-MODIS. *Remote Sens. Environ.* **1997**, *59*, 440–451. [CrossRef]
32. Huete, A.; Didan, K.; Miura, T.; Rodriguez, E.P.; Gao, X.; Ferreira, L.G. Overview of the Radiometric and Biophysical Performance of the MODIS Vegetation Indices. *Remote Sens. Environ.* **2002**, *83*, 195–213. [CrossRef]
33. Xiao, X.; Braswell, B.; Zhang, Q.; Boles, S.; Frolking, S.; Moore, B. Sensitivity of Vegetation Indices to Atmospheric Aerosols: Continental-Scale Observations in Northern Asia. *Remote Sens. Environ.* **2003**, *84*, 385–392. [CrossRef]
34. Matsushita, B.; Yang, W.; Chen, J.; Onda, Y.; Qiu, G. Sensitivity of the Enhanced Vegetation Index (EVI) and Normalized Difference Vegetation Index (NDVI) to Topographic Effects: A Case Study in High-Density Cypress Forest. *Sensors* **2007**, *7*, 2636–2651. [CrossRef] [PubMed]
35. Pizarro Gavilán, M. LandTrendr-based Vegetation Changes in Spain (1984-present). 2024. Available online: https://landtrend.csic.es/ltr-vegchanges/ (accessed on 2 February 2026).
36. Zhu, Z.; Woodcock, C.E. Object-Based Cloud and Cloud Shadow Detection in Landsat Imagery. *Remote Sens. Environ.* **2012**, *118*, 83–94. [CrossRef]
37. White, J.C.; Wulder, M.A.; Hobart, G.W.; Luther, J.E.; Hermosilla, T.; Griffiths, P.; Coops, N.C.; Hall, R.J.; Hostert, P.; Dyk, A.; et al. Pixel-Based Image Compositing for Large-Area Dense Time Series Applications and Science. *Can. J. Remote Sens.* **2014**, *40*, 192–212. [CrossRef]
38. Gorelick, N.; Hancher, M.; Dixon, M.; Ilyushchenko, S.; Thau, D.; Moore, R. Google Earth Engine: Planetary-Scale Geospatial Analysis for Everyone. *Remote Sens. Environ.* **2017**, *202*, 18–27. [CrossRef]
39. Joiner, J.; Yoshida, Y.; Zhang, Y.; Duveiller, G.; Jung, M.; Lyapustin, A.; Wang, Y.; Tucker, C.J. Estimation of Terrestrial Global Gross Primary Production (GPP) with Satellite Data-Driven Models and Eddy Covariance Flux Data. *Remote Sens.* **2018**, *10*, 1346. [CrossRef]

40. Fritts, H.C. *Tree Rings and Climate*; Academic Press: London, UK; New York, NY, USA, 1976.
41. Larsson, L.A.; Larsson, P.O. *CDendro and CooRecorder*; v. 9.8.1; Cybis Elektronik and Data AB: Saltsjöbaden, Sweden, 2022.
42. Holmes, R.L. Computer-Assisted Quality Control in Tree-Ring Dating and Measurement. *Tree-Ring Bull.* **1983**, *43*, 69–78.
43. Biondi, F.; Qeadan, F. A Theory-Driven Approach to Tree-Ring Standardization: Defining the Biological Trend from Expected Basal Area Increment. *Tree-Ring Res.* **2008**, *64*, 81–96.
44. Bunn, A.G. A dendrochronology program library in R (dplR). *Dendrochronologia* **2008**, *26*, 115–124. [CrossRef]
45. Bunn, A.G. Statistical and visual crossdating in R using the dplR library. *Dendrochronologia* **2010**, *28*, 251–258. [CrossRef]
46. Bunn, A.; Korpela, M.; Biondi, F.; Campelo, F.; Klesse, S.; Mérian, P.; Qeadan, F.; Zang, C.; Buras, A.; Cecile, A.; et al. dplR: Dendrochronology Program Library in R. 2025. Available online: https://cran.r-project.org/web/packages/dplR/index.html (accessed on 6 May 2026).
47. Lloret, F.; Keeling, E.; Sala, A. Components of tree resilience: Effects of successive low-growth episodes in old ponderosa pine forests. *Oikos* **2011**, *120*, 1909–1920. [CrossRef]
48. R Core Team. R: A Language and Environment for Statistical Computing. 2025. Available online: https://www.R-project.org/ (accessed on 6 May 2026).
49. Camarero, J.J.; Gazol, A.; Valeriano, C.; Colangelo, M.; Pizarro, M.; González de Andrés, E.; Pëto, A. Decoding hotter-drought impacts on canopy activity and tree growth to diagnose forest die-off. *Agric. For. Meteorol.* **2026**, *386*, 111238. [CrossRef]
50. Aussenac, G. Ecology and Ecophysiology of Circum-Mediterranean Firs in the Context of Climate Change. *Ann. For. Sci.* **2002**, *59*, 823–832. [CrossRef]
51. Castruita-Esparza, L.U.; Silva, L.C.R.; Gómez-Guerrero, A.; Villanueva-Díaz, J.; Correa-Díaz, A.; Horwath, W.R. Coping With Extreme Events: Growth and Water-Use Efficiency of Trees in Western Mexico During the Driest and Wettest Periods of the Past One Hundred Sixty Years. *J. Geophys. Res. Biogeosciences* **2019**, *124*, 3419–3431. [CrossRef]
52. Seftigen, K.; Frank, D.C.; Björklund, J.; Babst, F.; Poulter, B. The climatic drivers of normalized difference vegetation index and tree-ring-based estimates of forest productivity are spatially coherent but temporally decoupled in Northern Hemispheric forests. *Glob. Ecol. Biogeogr.* **2018**, *27*, 1352–1365. [CrossRef]
53. Mašek, J.; Tumajer, J.; Lange, J.; Kaczka, R.; Fišer, P.; Treml, V. Variability in Tree-Ring Width and NDVI Responses to Climate at a Landscape Level. *Ecosystems* **2023**, *26*, 1144–1157. [CrossRef]
54. Fang, O.; Zhang, Q.-B. Stress triggers tree-growth rebound in global forests. *Agric. For. Meteorol.* **2024**, *359*, 110285. [CrossRef]
55. Jiang, P.; Liu, H.; Piao, S.; Ciais, P.; Wu, X.; Yin, X.; Wang, H. Enhanced growth after extreme wetness compensates for post-drought carbon loss in dry forests. *Nat. Commun.* **2019**, *10*, 195. [CrossRef] [PubMed]
56. Liu, M.; Kannenberg, S.A.; Peñuelas, J.; Anderegg, W.R.L. A Global Comparison of Direct and Legacy Effects of Drought on Ecosystem Productivity. *Ecol. Lett.* **2026**, *29*, e70390. [CrossRef]